Ultrasound in Med. & Biol., Vol. 47, No. 2, pp. 279–287, 2021

0301-5629/$ - see front matter

https://doi.org/10.1016/j.ultrasmedbio.2020.10.007

● *Original Contribution*

CLINICAL UTILITY OF QUALITATIVE ELASTOGRAPHY USING ACOUSTIC RADIATION FORCE IMPULSE FOR DIFFERENTIATING BENIGN FROM MALIGNANT SALIVARY GLAND TUMORS

ERIKO MATSUDA, TAKAHIRO FUKUHARA, RYOHEI DONISHI, KENKICHIRO TAIRA, SATOSHI KOYAMA, TSUYOSHI MORISAKI, KAZUNORI FUJIWARA, and HIROMI TAKEUCHI
Department of Otolaryngology–Head and Neck Surgery, Tottori University Faculty of Medicine, Yonago, Japan

(*Received* 5 *August* 2020; *revised* 7 *October* 2020; *in final from* 12 *October* 2020)

Abstract—The goal of the work described here was to evaluate the utility of acoustic radiation force impulse (ARFI) imaging, a novel elastography technique, for differentiating benign from malignant salivary gland tumors. With the use of conventional strain elastography (SE) and ARFI imaging with a four-pattern scoring system, 185 tumors were examined (163 benign/22 malignant). When a score of ≥3 was used to define malignancy, the sensitivity, specificity and accuracy were higher for ARFI imaging (77.3%, 63.8% and 65.4%, respectively) than for conventional SE (54.5%, 56.4% and 56.2%, respectively). ARFI imaging findings revealed that most (92%) Warthin tumors, but only 24% of pleomorphic adenomas, were benign (score: 1 or 2). Attenuation of acoustic push pulses made it difficult to determine the stiffness of malignant tumors in the deep parotid lobes. Thus, ARFI imaging is a useful tool for screening Warthin tumors and exhibits high sensitivity for malignant tumors of salivary glands, other than deep parotid lobe tumors. (E-mail: eriko0521@hotmail.co.jp)

Key Words: **Ultrasonography, Elastography, Acoustic radiation force impulse, Acoustic radiation force impulse imaging, Salivary gland tumor, Parotid, Submandibular.**

INTRODUCTION

Ultrasonography (US) and magnetic resonance imaging (MRI) are the primary imaging techniques used to evaluate salivary gland tumors (Izzo et al. 2006; Burke et al. 2011). US is more advantageous than MRI for multiple reasons: It provides real-time data, is cost-effective and is highly versatile. In addition, US equipment has advanced dramatically in recent years and is now capable of evaluating finer blood flow and stiffness in the target tissues. Consequently, US application in the diagnosis of salivary gland tumors has elicited ongoing interest. However, the accuracy of a US-based diagnosis depends on the examiner's experience and diagnostic skills (Choi et al. 2010; Kim et al. 2010). These examinations are highly subjective and complicated by the presence of many evaluation items, such as shape, boundary, internal structure and homogeneity.

Address correspondence to: Eriko Matsuda, Department of Otolaryngology–Head and Neck Surgery, Tottori University Faculty of Medicine, Yonago 683-8504, Japan. E-mail: eriko0521@hotmail.co.jp

Elastography is a simple technique that involves specific evaluation of tissue stiffness (*i.e.,* softness or hardness). However, during conventional strain elastography (SE) using manual compression, tissue stiffness is expressed as a color map that changes dynamically depending on the variation in manual compression. This necessitates the selection of a suitable image from changing data. Thus, the accuracy of conventional SE examination depends on the examiner's experience level and predisposition for image selection (Westerland and Howlett 2012). In fact, the diagnostic accuracy of conventional SE for differentiating benign and malignant salivary gland tumors varies from 55.4%–94.0% in several published reports (Bhatia et al. 2010; Dumitriu et al. 2011; Celebi and Mahmutoglu 2013; Li et al. 2016; Cortcu et al. 2018; Karaman et al. 2019).

Recently, acoustic radiation force impulse (ARFI) imaging, a novel elastographic technique that uses acoustic compression, has been applied in clinical practice. Unlike conventional SE, ARFI imaging eliminates the examiner's subjectivity when selecting an image

because only one image is obtained for each acoustic compression. Furthermore, although conventional SE measures strain on the tissue under manual compression using the whole probe, ARFI imaging measures displacement by evaluating the detailed differences in tissue stiffness in response to fine compression, utilizing an acoustic push pulse. In fact, ARFI imaging has been described in the literature as being superior to conventional SE when differentiating between benign and malignant tumors in regions of the breast and thyroid gland (Tozaki et al. 2011; Xu et al. 2014; Fukuhara et al. 2018). This study aimed to elucidate the utility of ARFI imaging in differentiating benign from malignant salivary gland tumors.

METHODS

Patients

Consecutive patients who visited the Department of Otorhinolaryngology−Head and Neck Surgery of Tottori University Hospital between August 2014 and August 2019 were enrolled in the study if they met the following inclusion criteria: They had undergone examinations using US; received cytologic or pathologic confirmation of salivary gland tumor after the specimen examination; and received a diagnosis of a primary salivary gland tumor. Patients were excluded when the histologic type could not be diagnosed, or if complete US and elastography data were not available, or when the case involved a recurrence.

This retrospective study was approved by the Ethics Review Board of the Tottori University Faculty of Medicine. Informed consent was obtained from all participants. All procedures were conducted in accordance with the Declaration of Helsinki of 1975, as revised in 2013.

Procedures

Two head and neck surgeons and one sonographer performed all patient examinations. One surgeon had more than 10 and 5 y of experience in performing salivary gland examinations using US and elastography, respectively. The other surgeon had more than 5 y of experience using US and elastography in performing salivary gland examinations. The sonographer had more than 5 y of experience in utilizing US and elastography in the examination of the salivary glands.

Ultrasound systems

Ultrasound examinations were performed using an ACUSON S2000 ultrasound system (Siemens Healthineers, Mountain View, CA, USA), containing a 4- to 9-MHz or 14-MHz linear transducer for B-mode scans and a 4- to 9-MHz transducer for elastography.

Ultrasonographic examination

All patients underwent examinations of the bilateral parotid, submandibular and sublingual glands, in the supine position. The tumors were evaluated using B-mode US. The diameter of each tumor was measured at the widest region.

Elastography

For elastography, conventional SE and ARFI imaging were performed. The transducer was held motionless and in light contact with the skin over the salivary gland. A region of interest was placed surrounding the tumor that included the salivary gland parenchyma.

Conventional SE

eSie Touch elasticity imaging was used for conventional SE. This US application display depicts the stiff tissue regions, soft tissue regions and intermediate stiffness in blue, red and green, respectively. We adopted the recommendations from Siemens for indicating eSie Touch elasticity imaging quality, including the use of SE images with a strain quality indicator >50 for the tumor (Shiina et al. 2015; Cosgrove et al. 2017). This system was applied three times at the same location. A four-pattern scoring system was used to grade the conventional SE images. This is the same system described in published reports on salivary gland tumors and the World Federation for Ultrasound in Medicine and Biology guidelines regarding the clinical use of elastography for the thyroid (Bhatia et al. 2010; Dumitriu et al. 2011; Cosgrove et al. 2017). In the four-pattern scoring system, scores of 1−4 represent tumors as follows: 1 = entirely green; 2 = mostly green with some blue areas; 3 = mostly blue; 4 = entirely blue (Fig. 1). The images were scored separately by a board-certified fellow of the Japan Society of Ultrasonics in Medicine (JSUM) and a JSUM-registered medical sonographer. Both of them were blinded to the histologic findings and tumor diagnoses. When there were discrepancies between the scores, a final decision was reached by consensus after discussion. Concordance of the conventional SE imaging scores of the three images was evaluated for each tumor. Thereafter, the percentage of tumors with matching scores on the three images was determined.

ARFI imaging

The Virtual Touch imaging system was used for ARFI imaging. This system was applied three times at the same location. ARFI images were assessed using a four-pattern gray-scale scoring system, with scores of 1−4 indicating a tumor as follows: 1 = white or white-honeycomb colored; 2 = light gray or mainly light gray mixed with white areas; 3 = mostly black or dark gray with some white or light gray areas; 4 = entirely black or dark gray (Fig. 2).

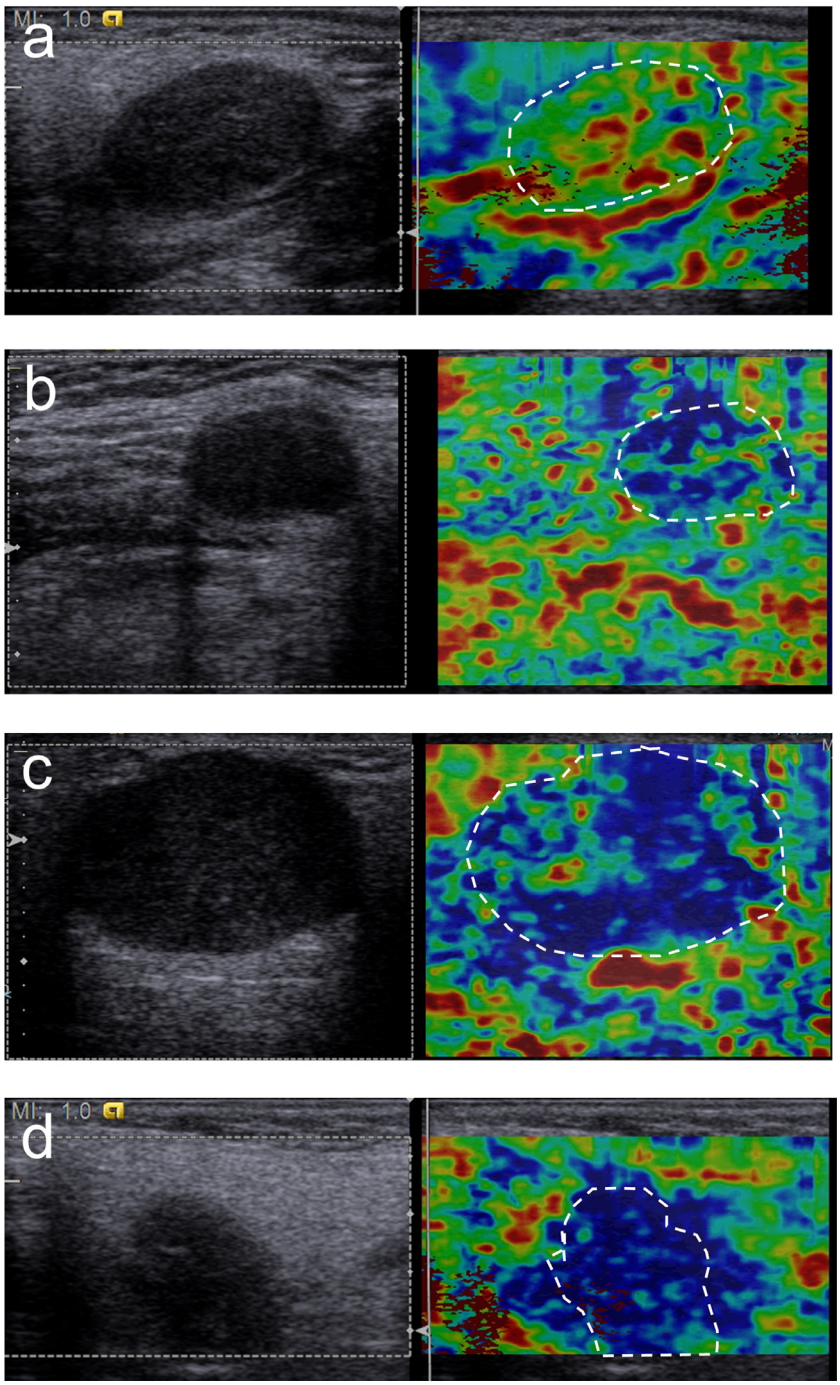

Fig. 1. Four-pattern scoring system of conventional strain elastography. (a) A score of 1 indicates a tumor that is entirely green. (b) A score of 2 indicates a tumor that is mostly green with some blue areas. (c) A score of 3 indicates a tumor that is mostly blue with some green areas. (d) A score of 4 indicates a tumor that is entirely blue.

The images were scored separately by a JSUM board-certified fellow and a JSUM-registered medical sonographer, who were blinded to the histologic findings and diagnoses of the tumors. When there were discrepancies between the scores, a final decision was reached by consensus after discussion. Concordance of the ARFI imaging scores of the three images was evaluated for each tumor. Thereafter, the percentage of tumors with matching scores on the three images was determined. When two images matched and one image differed, the score of the two matches was chosen. When all three imaging scores differed, the score was considered indeterminate.

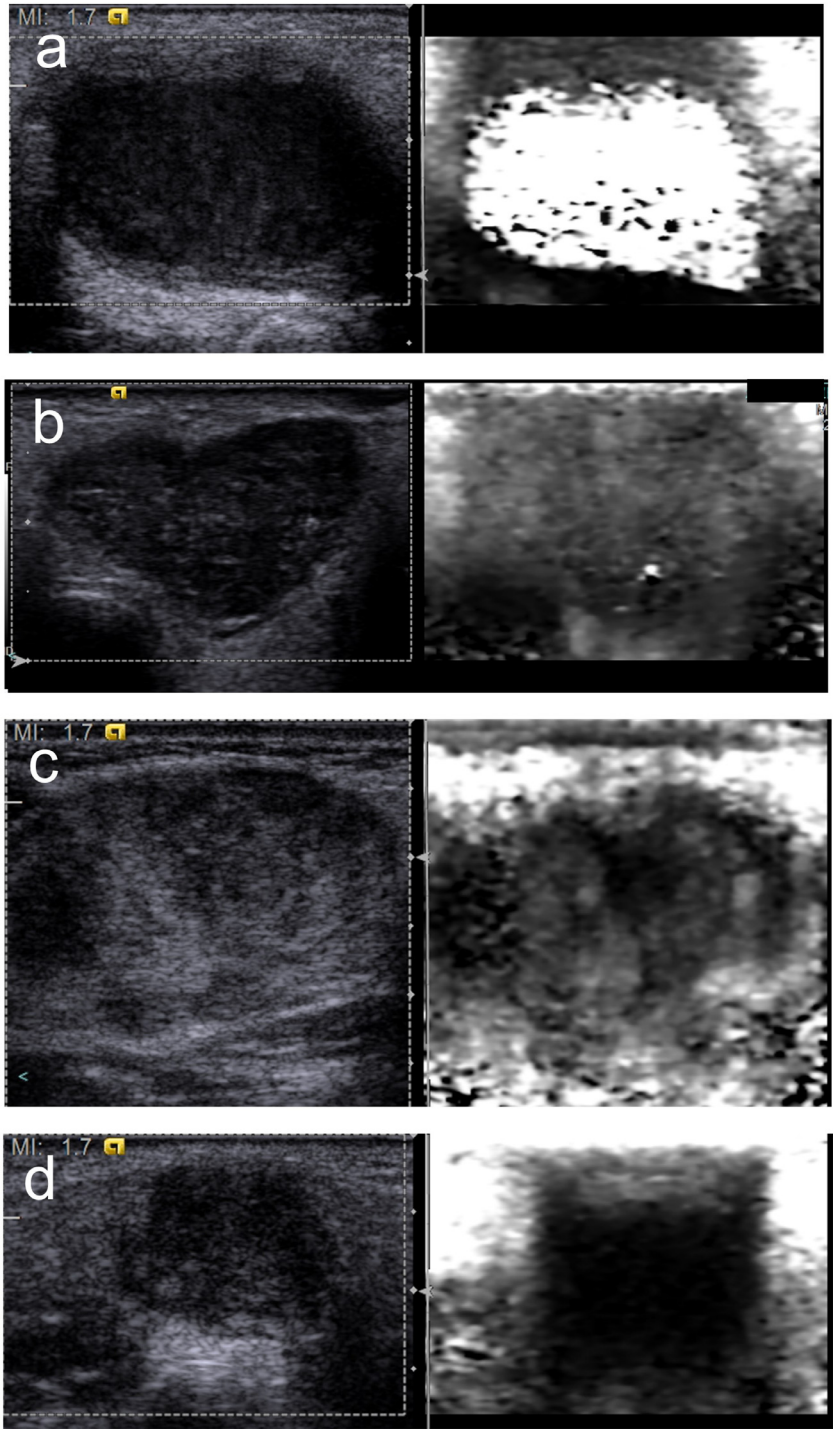

Fig. 2. Four-pattern scoring system of acoustic radiation force impulse imaging. (a) A score of 1 indicates a tumor that is white or white-honeycomb colored. (b) A score of 2 indicates a tumor that is light gray or mainly light gray and mixed with white areas. (c) A score of 3 indicates a tumor that is mostly black or dark gray, with some white or light gray areas. (d) A score of 4 indicates a tumor that is entirely black or dark gray.

Parotid glands have a high fat content and are, thus, hyper-echoic, with marked attenuation of US waves. Consequently, tumors in the deep parotid lobe are often difficult to be detected from gray-scale images during a US assessment (Bialek et al. 2006). Therefore, we focused only on parotid gland tumors and divided these cases into those with superficial lobes and those with deep lobes. Surgical findings and MRI were used to

assign the tumors into one of the two groups. In surgical cases, the findings were reviewed, and the tumors were judged to be deep lobe tumors when they were deeper than the facial nerve. In all other cases, the tumors were judged to be deep lobe tumors when they were deeper than the position of the parotid duct or the retromandibular vein, as observed in MRI findings (Imaizumi et al. 2009). Thereafter, the diagnostic accuracies of conventional SE and ARFI imaging procedures were compared. In addition, the reproducibility of conventional SE and ARFI imaging was evaluated.

Statistical analysis

Analysis was performed using SPSS Statistics for Windows, Version 25 (IBM Corporation, Armonk, NY, USA). Descriptive statistics were used to summarize the characteristics of the study group and were expressed as the mean ± standard deviation. The diameters of benign and malignant tumors were compared using the Mann−Whitney *U*-test. Elastographic scores were dichotomized using a cutoff value between 2 and 3 to distinguish the benign and malignant tumors. Sensitivity, specificity and diagnostic accuracy of conventional SE and ARFI imaging for malignant tumors were calculated using a χ^2-test. For all statistical tests, a p value <0.05 was considered to indicate statistical significance.

RESULTS

A total of 185 tumors found in 168 patients were included in the analysis (Fig. 3). Demographic data from the patients and basic characteristics of the salivary gland tumors are summarized in Table 1. The tumors corresponded to the following regions: parotid gland, 169; submandibular gland, 15; and sublingual gland, 1.

Table 1. Basic characteristics of the patients and salivary gland tumors

	Benign	Malignant	*p* value
Patients			
Number	147	21	
Sex (male/female)	89/58	14/7	
Age	62.8 ± 14.4*	62.7 ± 14.9	
Tumors			
Number	163	22	
Parotid/submandibular/sublingual	150/13/0	19/2/1	
Longest diameter (mm)	27.6 ± 12.1	31.5 ± 14.9	<0.001

* Mean ± standard deviation.

There were 163 and 22 benign and malignant tumors, respectively. Mean tumor sizes were 27.6 ± 12.1 and 31.5 ± 14.9 mm for the benign and malignant tumors, respectively. The benign tumors included 87 Warthin tumors, 68 pleomorphic adenomas, 3 basal cell adenomas, 3 oncocytomas, 1 myoepithelioma and 1 cystadenoma (Table 2). The malignant tumors included 5 mucoepidermoid carcinomas, 4 salivary duct carcinomas, 4 squamous cell carcinomas, 3 epithelial myoepithelial carcinomas, 2 carcinoma *ex* pleomorphic adenomas, 2 adenoid cystic carcinomas, 1 myoepithelial carcinoma and 1 large cell undifferentiated carcinoma.

Accuracy of differentiation between benign and malignant tumors

Table 3 lists the scores determined *via* conventional SE and ARFI imaging. For benign tumors determined by conventional SE, scores of 1, 2, 3 and 4 were recorded in 38 (23.3%), 54 (33.1%), 47 (28.8%) and 24 (14,7%) cases, respectively. For malignant tumors, conventional SE scores of 1, 2, 3 and 4 were recorded in 2 (9.1%), 8 (36.4%), 4 (18.1%) and 8 (36.4%) cases, respectively.

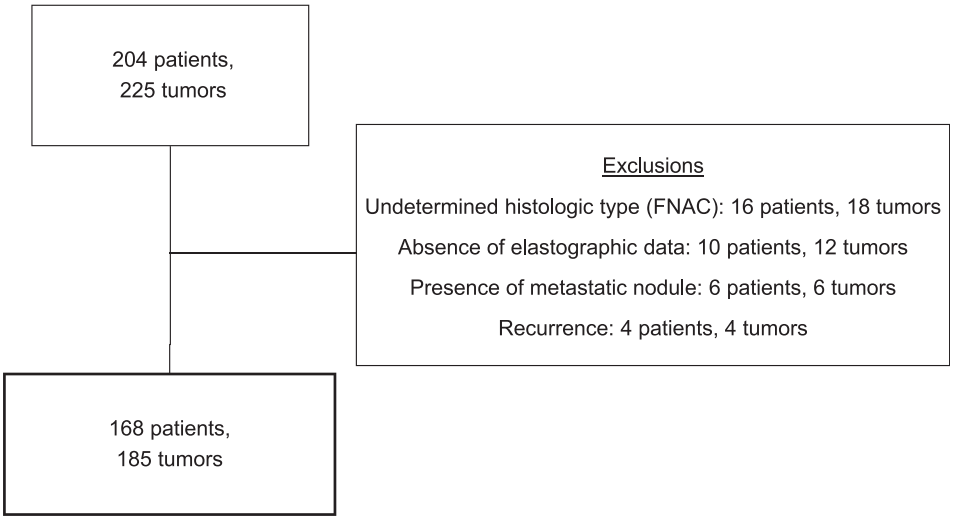

Fig. 3. Flowchart of patient selection for this study. FNAC = fine-needle aspiration cytology.

Table 2. Distribution of the histologic types of salivary gland tumors

Histologic type	No.	Parotid/submandibular/sublingual
Benign tumors		
Warthin tumor	87	87/0/0
Pleomorphic adenoma	68	55/13/0
Basal cell adenoma	3	3/0/0
Oncocytoma	3	3/0/0
Myoepithelioma	1	1/0/0
Cystadenoma	1	1/0/0
Malignant tumors		
Mucoepidermoid carcinoma	5	4/1/0
Salivary duct carcinoma	4	4/0/0
Squamous cell carcinoma	4	4/0/0
Epithelial myoepithelial carcinoma	3	3/0/0
Carcinoma *ex* pleomorphic adenoma	2	1/1/0
Adenoid cystic carcinoma	2	1/0/1
Myoepithelial carcinoma	1	1/0/0
Large cell undifferentiated carcinoma	1	1/0/0

Table 3. Scores for conventional SE and ARFI imaging

	Conventional SE score			
	1	2	3	4
Benign	38	54	47	24
Malignant	2	8	4	8
	ARFI imaging score			
	1	2	3	4
Benign	11	93	37	22
Malignant	0	5	6	11

SE strain elastography; ARFI = acoustic radiation force impulse.

When malignancy was defined using a conventional SE score ≥3, the sensitivity, specificity and accuracy were 54.5%, 56.4% and 56.2%, respectively.

For benign tumors, ARFI imaging scores of 1−4 were recorded. In 11 (6.7%), 93 (57.1%), 37 (22.7%) and 22 (13.4%) cases, the scores were 1, 2, 3 and 4, respectively. For malignant tumors, ARFI imaging scores of 2, 3 and 4 were recorded in 5 (22.7%), 6 (27.3%) and 11 (50.0%) cases, respectively. By use of the aforementioned results, it was determined that the sensitivity and specificity were the highest when a score of 3 on ARFI imaging was used as the cutoff value to classify malignancy. When malignancy was defined using an ARFI imaging score ≥3, the sensitivity, specificity and accuracy were 77.3%, 63.8% and 65.4%, respectively.

Comparing reproducibility of scores between conventional SE and ARFI imaging

Of the 185 cases considered, 27 were excluded because conventional SE was performed only once. In the remaining 158 cases, the score match rates for all three images of conventional SE were 83.5% (132 cases).

In contrast, among the 185 cases, the score match rates for all three images of ARFI imaging were as high as 96.2% (178 cases). In 7 cases, one of the three images had a different score. There were no cases in which all three images had different scores.

Histologic review of ARFI imaging scores

The ARFI imaging scores for each histologic type are outlined in Table 4. Warthin tumors and pleomorphic adenomas accounted for 96% of all benign tumors. Almost all Warthin tumors (92.0%) and only 23.5% of pleomorphic adenomas received a score of 1 or 2. The most malignant tumors (77.3%) received a score of 3 or 4 on ARFI imaging. Among the malignant tumors, 2 adenoid cystic carcinomas, 2 mucoepidermoid carcinomas and 1 epithelial myoepithelial carcinoma received a score of 2.

Salivary gland cancers were stratified into low/intermediate and high malignancy groups, according to the pathologic grade. The results from the ARFI imaging score comparison between the groups are summarized in Table 5. As the ARFI imaging scores of pleomorphic adenomas were high, it was difficult to distinguish the low/intermediate and high malignancy groups from pleomorphic adenoma. Four cases of low/intermediate malignancy of the parotid deep lobe exhibited a benign pattern of ARFI imaging with a score of 2. In addition, a sublingual cancer exhibited a benign pattern of ARFI imaging with a score of 2. The pre-operative pathology of the sublingual cancer indicated internal necrosis.

Review of ARFI imaging scores with respect to tumor location in parotid gland

The ARFI imaging scores with respect to tumor location in the parotid gland are listed in Table 6. Among

Table 4. Results of ARFI imaging with respect to histologic type

Histologic type	ARFI imaging score			
	1	2	3	4
Benign tumors				
Warthin tumor	7	73	7	0
Pleomorphic adenoma	3	13	30	22
Other tumors	1	7	0	0
Malignant tumors				
Mucoepidermoid carcinoma	0	2	2	1
Salivary duct carcinoma	0	0	0	4
Squamous cell carcinoma	0	0	0	4
Epithelial myoepithelial carcinoma	0	1	2	0
Carcinoma *ex* pleomorphic adenoma	0	0	0	2
Adenoid cystic carcinoma	0	2	0	0
Myoepithelial carcinoma	0	0	0	1
Large cell undifferentiated carcinoma	0	0	0	1

ARFI = acoustic radiation force impulse.

Table 5. Results of ARFI imaging of malignant tumors according to histologic grades

Gland	Histologic grade							
	Low/intermediate (n = 10)				High (n = 12)			
	ARFI imaging score				ARFI imaging score			
	1	2	3	4	1	2	3	4
Parotid gland								
Superficial lobe	0	0	4	0	0	0	2	8
Deep lobe	0	4	0	0	0	0	0	1
Submandibular gland	0	0	0	1	0	0	0	1
Sublingual gland	0	1	0	0	0	0	0	0

ARFI = acoustic radiation force impulse.

the 169 parotid tumors, 142 (128 benign and 14 malignant) and 27 (22 benign and 5 malignant) were located in the superficial and the deep parotid lobe, respectively. Regarding the diagnostic accuracy of the ARFI imaging score in predicting the malignancy of tumors in the superficial parotid lobe, the sensitivity, specificity and accuracy were 100%, 66.4% and 69.7%, respectively. In contrast, the corresponding sensitivity, specificity and accuracy were 20%, 77.3% and 66.7%, respectively, for tumors in the deep parotid lobe.

DISCUSSION

In our elastography analysis, ARFI imaging yielded slightly higher sensitivity, specificity and accuracy than conventional SE.

The diagnostic accuracy of conventional SE in this study tended to be lower than that reported previously (Cortcu et al. 2018; Karaman et al. 2019). The eSie Touch imaging used in this study as conventional SE was selected on the basis of numerical parameters (strain quality indicator >50). However, previous studies, with diagnostic accuracies >80%, may have had image selection bias. It is also possible that the wide range of diagnostic accuracy of conventional SE published in previous reports (55.4%−94.0%) might have been caused by image selection bias and the experience level and skill of examiners (Bhatia et al. 2010; Dumitriu et al. 2011; Celebi and Mahmutoglu 2013; Li et al. 2016; Cortcu et al. 2018; Karaman et al. 2019).

Table 6. Results of ARFI imaging scores with respect to tumor location in the parotid gland

Status	ARFI imaging score			
	1	2	3	4
		Superficial lobe		
Benign	9	76	26	17
Malignant	0	0	6	8
		Deep lobe		
Benign	2	15	2	3
Malignant	0	4	0	1

ARFI = acoustic radiation force impulse.

In ARFI imaging, the selection bias is removed because only one image is received for each examination. Furthermore, as the manual compression technique is not required, there are no differences based on the examiner's ability. ARFI imaging was also found to be highly reproducible in our study, with high concordance rates (96.2%) of the three measurement scores. Therefore, we concluded that, from the perspective of the examiner, ARFI imaging was easier to use than conventional SE.

The diagnostic accuracy of ARFI imaging, compared with conventional SE, was not as high as expected. ARFI imaging analysis according to histologic classification revealed that among the benign tumors, almost all Warthin tumors (92.0%) received a benign score (1 or 2). In contrast, only 23.5% of pleomorphic adenomas received a benign score. The others received malignant scores (3 or 4). Bhatia et al. (2010, 2013) reported the difficulty in determining the malignancy of pleomorphic adenoma by elastography (conventional SE) and noted that this challenge reduced diagnostic accuracy. Yerli et al. (2012) reported that pleomorphic adenomas were more difficult to classify than other benign tumors because of the mesenchyme-like component of pleomorphic adenomas. Thus, pleomorphic adenomas are considered to be a source of the decreased specificity and diagnostic accuracy of ARFI imaging for differentiating malignant tumors in our study. The results were reviewed in terms of histologic grade and revealed that ARFI imaging could not distinguish pleomorphic adenomas from malignancy in the current setting.

In contrast, most malignant tumors (77%) received a malignant score (3 or 4) on ARFI imaging, although 5 cases received a benign score (1 or 2). In these 5 cases, no fixed tendency was observed in an examination of malignant histologic type. However, 4 tumors were located in the deep lobe of the parotid gland, and 1 tumor was located in the submandibular gland. The acoustic push pulse for ARFI imaging may be attenuated at these deep sites, hindering appropriate imaging. For this reason, we placed our focus on the superficial and the deep lobes of the parotid gland.

The parotid gland tumors in the superficial and deep lobes were examined separately. For those in the superficial lobe, the sensitivity for differentiating malignant tumors was 100%. In contrast, for tumors in the deep lobes, the sensitivity was 20%, and results for most malignant tumors were false negative. This poor sensitivity of ARFI imaging in the deep parotid lobes was attributed to a small displacement difference between the harder and softer areas, caused by the inability of attenuated acoustic push pulses to reach the deep parotid lobe and insufficient acoustic compression.

In fact, acoustic pulses are strongly attenuated at the deep lobes of the parotid gland. B-Mode US images of the deep lobe are not clear because the parotid parenchyma is rich in fatty components (Bialek et al. 2006). We believe that when the acoustic push pulse can be adjusted to the appropriate intensity, it may be possible to differentiate salivary gland tumors that could not be previously performed.

Although ARFI imaging does not distinguish pleomorphic adenomas and salivary gland carcinomas in this setting, this disadvantage would affect few treatment regimens for salivary gland tumors. Unlike Warthin tumors, pleomorphic adenomas are associated with the possibility of malignant transformation, and their presence is an indication for surgery (Renehan et al. 1996; Park et al. 2012). Therefore, ARFI imaging is considered useful for differentiating malignant and benign Warthin tumors, for which a wait-and-see approach to treatment is applied. In summary, unlike conventional SE, ARFI imaging is an expedient tool in screening for salivary gland tumors, as there is no need for compression technique or image selection. In future studies, it would be necessary to examine the usefulness of ARFI imaging combined with other methods, such as B-mode and Doppler, for diagnosis.

This study had several limitations. First, there were more patients with benign than with malignant tumors. However, a previous investigation reported a malignancy rate of 20% among salivary gland tumors, which was similar to our findings (Sentani et al. 2019). Second, pleomorphic adenomas often presented with a false-positive pattern on ARFI imaging, and thus, the proportion of pleomorphic adenomas appearing in our participants might have affected the diagnostic accuracy. Third, the intensity of acoustic compression during ARFI imaging was not available, because it is a trade secret. Unfortunately, this meant that we could not examine its influence.

CONCLUSIONS

Compared with conventional SE, ARFI imaging has the advantage of high reproducibility (96.2%). The diagnostic accuracy of this technique for salivary gland malignancy is not inferior to that of conventional elastography. Furthermore, ARFI imaging may be useful for differentiating malignant from benign Warthin tumors that do not require surgery. It is important to note that among the benign tumors, pleomorphic adenomas often yielded a false-positive pattern in ARFI imaging in our study. When the diagnostic accuracy of ARFI imaging for differentiating benign and malignant parotid tumors was evaluated, the sensitivity was high for tumors in the superficial lobes but low for those in the deep lobes. This was attributed to acoustic push pulse attenuation. The power of the acoustic push pulse needs to be adjusted to improve the diagnostic accuracy of the salivary gland tumors when using ARFI imaging.

Acknowledgments—This work was supported by a Grant-in-Aid for Young Scientists (JP19 K18730) from the Japan Society for the Promotion of Science.

Conflict of interest disclosure—The authors declare no conflicts of interest associated with this article.

REFERENCES

Bhatia KS, Rasalkar DD, Lee YP, Wong KT, King AD, Yuen HY, Ahuja AT. Evaluation of real-time qualitative sonoelastography of focal lesions in the parotid and submandibular glands: Applications and limitations. Eur Radiol 2010;20:1958–1964.

Bhatia KS, Lee YY, Yuen EH, Ahuja AT. Ultrasound elastography in the head and neck: Part II. Accuracy for malignancy. Cancer Imaging 2013;13:260–276.

Bialek EJ, Jakubowski W, Zajkowski P, Szopinski KT, Osmolski A. US of the major salivary glands: Anatomy and spatial relationships, pathologic conditions, and pitfalls. Radiographics 2006;26:745–763.

Burke CJ, Thomas RH, Howlett D. Imaging the major salivary glands. Br J Oral Maxillofac Surg 2011;49:261–269.

Celebi I, Mahmutoglu AS. Early results of real-time qualitative sonoelastography in the evaluation of parotid gland masses: A study with histopathological correlation. Acta Radiol 2013;54:35–41.

Choi SH, Kim EK, Kwak JY, Kim MJ, Son EJ. Interobserver and intraobserver variations in ultrasound assessment of thyroid nodules. Thyroid 2010;20:167–172.

Cortcu S, Elmali M, Tanrivermis Sayit A, Terzi Y. The role of real-time sonoelastography in the differentiation of benign from malignant parotid gland tumors. Ultrasound Q 2018;34:52–57.

Cosgrove D, Barr R, Bojunga J, Cantisani V, Chammas MC, Dighe M, Vinayak S, Xu JM, Dietrich CF. WFUMB guidelines and recommendations on the clinical use of ultrasound elastography: Part 4. Thyroid. Ultrasound Med Biol 2017;43:4–26.

Dumitriu D, Dudea S, Botar-Jid C, Baciut M, Baciut G. Real-time sonoelastography of major salivary gland tumors. AJR Am J Roentgenol 2011;197:W924–W930.

Fukuhara T, Matsuda E, Donishi R, Koyama S, Miyake N, Fujiwara K, Takeuchi H. Clinical efficacy of novel elastography using acoustic radiation force impulse (ARFI) for diagnosis of malignant thyroid nodules. Laryngoscope Investig Otolaryngol 2018;3:319–325.

Imaizumi A, Kuribayashi A, Okochi K, Ishii J, Sumi Y, Yoshino N, Kurabayashi T. Differentiation between superficial and deep lobe parotid tumors by magnetic resonance imaging: Usefulness of the parotid duct criterion. Acta Radiol 2009;50:806–811.

Izzo L, Casullo A, Caputo M, Costi U, Guerrisi A, Stasolla A, Basso L, Marini M, De Toma G. Space occupying lesions of parotid gland: Comparative diagnostic imaging and pathological analysis of echo color/power Doppler and of magnetic resonance imaging. Acta Otorhinolaryngol Ital 2006;26:147–153.

Karaman CZ, Başak S, Polat YD, Ünsal A, Taşkın F, Kaya E, Günel C. The role of real-time elastography in the differential diagnosis of salivary gland tumors. J Ultrasound Med 2019;38:1677–1683.

Kim SH, Park CS, Jung SL, Kang BJ, Kim JY, Choi JJ, Kim YI, Oh JK, Oh JS, Kim H, Jeong SH, Yim HW. Observer variability and the performance between faculties and residents: US criteria for benign and malignant thyroid nodules. Korean J Radiol 2010;11:149–155.

Li C, Zhang C, Li N, Li J. Compression real-time elastography for evaluation of salivary gland lesions: A meta-analysis. J Ultrasound Med 2016;35:999–1007.

Park GC, Cho KJ, Kang J, Roh JL, Choi SH, Kim SY, Nam SY. Relationship between histopathology of pleomorphic adenoma in the parotid gland and recurrence after superficial parotidectomy. J Surg Oncol 2012;106:942–946.

Renehan A, Gleave EN, McGurk M. An analysis of the treatment of 114 patients with recurrent pleomorphic adenomas of the parotid gland. Am J Surg 1996;172:710–714.

Sentani K, Ogawa I, Ozasa K, Sadakane A, Utada M, Tsuya T, Kajihara H, Yonehara S, Takeshima Y, Yasui W. Characteristics of 5015 salivary gland neoplasms registered in the Hiroshima Tumor Tissue Registry over a period of 39 years. J Clin Med 2019;8:566.

Shiina T, Nightingale KR, Palmeri ML, Hall TJ, Bamber JC, Barr RG, Castera L, Choi BI, Chou YH, Cosgrove D, Dietrich CF, Ding H, Amy D, Farrokh A, Ferraioli G, Filice C, Friedrich-Rust M, Nakashima K, Schafer F, Sporea I, Suzuki S, Wilson S, Kudo M. WFUMB guidelines and recommendations for clinical use of ultrasound elastography: Part 1. Basic principles and terminology. Ultrasound Med Biol 2015;41:1126–1147.

Tozaki M, Isobe S, Fukuma E. Preliminary study of ultrasonographic tissue quantification of the breast using the acoustic radiation force impulse (ARFI) technology. Eur J Radiol 2011;80: e182–e187.

Westerland O, Howlett D. Sonoelastography techniques in the evaluation and diagnosis of parotid neoplasms. Eur Radiol 2012;22:966–969.

Xu JM, Xu XH, Xu HX, Zhang YF, Zhang J, Guo LH, Liu LN, Liu C, Zheng SG. Conventional US, US elasticity imaging, and acoustic radiation force impulse imaging for prediction of malignancy in thyroid nodules. Radiology 2014;272:577–586.

Yerli H, Eski E, Korucuk E, Kaskati T, Agildere AM. Sonoelastographic qualitative analysis for management of salivary gland masses. J Ultrasound Med 2012;31:1083–1089.